Local Environment of Strontium Cations Activating NaTaO3 Photocatalysts

An, Longjie ; Sasaki, Takuro ; Weidler, Peter G. ; Woell, Christof ; Ichikuni, Nobuyuki ; Onishi, Hiroshi

(Citation)
ACS Catalysis,8(2):880-885

(Issue Date)
2018-02

(Resource Type)
journal article

(Version)
Version of Record

ACS Catalysis

Research Article

Cite This: ACS Catal. 2018, 8, 880−885

pubs.acs.org/acscatalysis

Local Environment of Strontium Cations Activating $NaTaO_3$ Photocatalysts

Longjie An,[†] Takuro Sasaki,[‡] Peter G. Weidler,[§] Christof Wöll,[§] Nobuyuki Ichikuni,[‡] and Hiroshi Onishi*[,†]

[†]Department of Chemistry, Graduate School of Science, Kobe University, Rokko-dai, Nada, Kobe, Hyogo 657-8501, Japan

[‡]Department of Applied Chemistry and Biotechnology, Graduate School of Engineering, Chiba University, Yayoi-cho, Inage, Chiba 263-8522, Japan

[§]Institute for Functional Interfaces, Karlsruhe Institute of Technology, Campus Nord, 76344 Eggenstein-Leopoldshafen, Germany

Supporting Information

ABSTRACT: Sodium tantalate, $NaTaO_3$, is one of the best semiconductors for photocatalytic water splitting and CO_2 reduction. Doping with metal cations is crucial for enhancing the quantum efficiency of the desired reactions. Nevertheless, details related to the doping of the host metal oxide and activation by guest metal cations are not sufficiently known. The most fundamental question concerns the increase in the quantum efficiency via doping with guest cations that are impurities in the host lattice. In this study, the local environment of Sr cations, which are the typically used guest cations in $NaTaO_3$, was characterized by extended X-ray absorption fine structure spectroscopy. The results reveal the presence of two Sr−O shells in the Sr-doped $NaTaO_3$ photocatalysts. The small shell with an unexpectedly short Sr−O bond length of 1.96 Å corresponds to SrO_6 octahedra embedded in the corner-shared network of TaO_6 octahedra. The other shell with a Sr−O bond length of 2.60 Å corresponds to SrO_{12} cuboctahedra with Sr cations at positions previously occupied by Na cations. Rietveld analysis of the X-ray diffraction data confirmed the formation of a $NaTaO_3$−$Sr(Sr_{1/3}Ta_{2/3})O_3$ solid solution to accommodate the two Sr−O shells in $NaTaO_3$ with no requirement for creating oxygen anion vacancies. Mechanisms for increasing the quantum efficiency via doping with Sr cations are discussed in the context of the revealed environment.

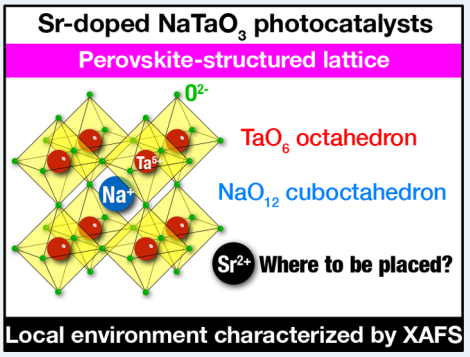

KEYWORDS: *photocatalysis, recombination, doping, X-ray absorption, Rietveld analysis, perovskite structure, solid solution, solar hydrogen*

1. INTRODUCTION

Sodium tantalate, $NaTaO_3$ is the semiconductor photocatalyst for highly efficient artificial photosynthesis. Kudo and co-workers used this perovskite-structured metal oxide for the overall water-splitting reaction. A quantum efficiency of greater than 50% has been reported for water splitting using $NaTaO_3$ doped with lanthanum.[1,2] Doping with alkaline-earth metal cations is effective in enhancing the efficiency as well.[3,4] The rate of H_2 production was 1.7 mmol h^{-1} on pristine $NaTaO_3$ and increased to 19.8, 9.5, 9.3, or 4.9 mmol h^{-1} via doping with La^{3+}, Sr^{2+}, Ba^{2+} or Ca^{2+} cations, respectively.[5] Doping with two metal cations[6−10] has been subsequently examined for the sensitization of this wide-band-gap semiconductor to visible light. Currently, studies are being extensively carried out on double doping with one cation and one anion.[11−18] The photocatalytic reduction of CO_2 using pristine[19] and metal-doped $NaTaO_3$[20,21] also has been reported.

Doping with metal cations is crucial for the modification of $NaTaO_3$ photocatalysts, as demonstrated in the above-mentioned studies. Nevertheless, details related to the doping and activation of the host metal oxide for increased water splitting efficiency are not known. Since these cations are impurities in the crystalline host lattice, the increase in the quantum efficiency via doping with metal cations is the most fundamental question that needs to be answered. Recently, An and Onishi[22] challenged a received hypothesis that Na^+ cations in $NaTaO_3$ are simply doped with alkaline-earth metal cations. They proposed the formation of a $NaTaO_3$−$Sr(Sr_{1/3}Ta_{2/3})O_3$ solid solution in Sr-doped $NaTaO_3$ photocatalysts, in addition to similar solid solutions in Ca- and Ba-doped photocatalysts. Regularly separated 10 nm steps spontaneously appeared on the surface of $NaTaO_3$ particles doped with alkaline-earth metal cations,[4] as was observed on particles doped with lanthanum.[1] The lattice mismatch in a particle consisting of a Sr-rich solid-solution shell over a Sr-poor solid-solution core induced the steps at the surface.[22] The doping of Ta^{5+} cations with alkaline-earth metal cations has been further argued to be

Received: October 19, 2017
Revised: December 12, 2017
Published: December 18, 2017

DOI: 10.1021/acscatal.7b03567
ACS Catal. 2018, 8, 880−885

crucial to the enhanced quantum efficiency in the solid solution.

In their study,[22] the doping of Ta cations was evidenced by the symmetry-driven presence or absence of a Raman band. In this study, X-ray absorption fine structure (XAFS) spectroscopy and Rietveld analysis of the X-ray diffraction (XRD) data were utilized to determine the local environment of the Sr cations in $NaTaO_3$ photocatalysts. Extended X-ray absorption fine structure (EXAFS) should be useful for characterizing the metal cations embedded in $NaTaO_3$. Only one extended[23] and one near-edge[24] structure of La-doped photocatalysts have been reported to date.

$NaTaO_3$ exhibits a perovskite structure with a slightly distorted orthorhombic symmetry (*Pbnm*, a = 5.48 Å, b = 5.52 Å, c = 7.79 Å) at room temperature.[25] The orthorhombic cell comprises four $NaTaO_3$ units, and a cube with a side length of 3.89 Å, the volume of which corresponds to one-fourth of the orthorhombic cell volume, is assigned to one $NaTaO_3$ unit on average. In the average cubic unit cell, which is shown in Figure 1, Na cations at the A sites are coordinated to 12 O anions, affording NaO_{12} cuboctahedra. Tantalum cations at the B sites are at the centers of TaO_6 octahedra.

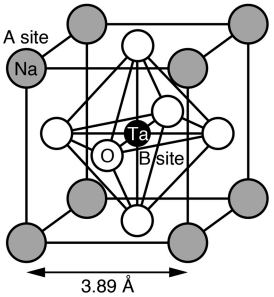

Figure 1. Average cubic unit cell of $NaTaO_3$ with Na^+ and Ta^{5+} cations at the A and B sites, respectively.

2. EXPERIMENTAL SECTION

2.1. Photocatalyst Preparation. Strontium-doped $NaTaO_3$ photocatalysts were prepared through a solid-state reaction. First, mixtures of Na_2CO_3 (99.8%, Kanto), Ta_2O_5 (99.99%, Rare Metallic Co. Ltd.), and $SrCO_3$ (99.9%, Kanto) were calcined in alumina crucibles at 1173 K for 1 h and then at 1423 K for 10 h according to methods reported previously.[1,3,22] The Sr/Ta ratio in the mixtures with a constant Na/Ta molar ratio of 1.05 was adjusted to 0, 2, 8, 20, and 50 mol %. Excess Na remaining in the calcined products was washed with water. Hereafter, the water-washed photocatalysts are denoted as NTO, Sr-NTO (2 mol %), Sr-NTO (8 mol %), Sr-NTO (20 mol %), and Sr-NTO (50 mol %). The concentrations of Sr in the photocatalysts were quantified as 0, 2.1, 8.3, 20.8, and 49.0 mol % by energy-dispersive X-ray fluorescence spectrometry (Shimadzu, EDX-720). A single perovskite-structured phase for NTO and each Sr-NTO was confirmed by XRD (Figure S1 in the Supporting Information) using a SmartLab diffractometer (Rigaku). Sr-NTO (50 mol %) was washed with an aqueous HCl solution (1 mol L^{-1}) for 10 min at room temperature and then washed with water until the pH of the washing fluid was maintained at 7. HCl-washed Sr-NTO (50 mol %) exhibited a decrease in the Sr concentration to 44.2 mol %. A small but finite decrease indicates that Sr-containing residue on the surface of Sr-NTO (50 mol %) does not show any X-ray diffraction.

2.2. X-ray Absorption Measurements. Absorption spectra at the Sr K-edge and Ta L_3-edge were recorded with a Si(111) double-crystal monochromator at BL-12C of the Photon Factory (Tsukuba, Japan). Measurement details have been added to the Supporting Information. Curve-fitting analysis of the extended fine structures was carried out using the IFEFFIT package including Athena and Artemis.[26]

2.3. XRD and Rietveld Analysis. Diffraction patterns for Rietveld analysis were recorded on a D8 Advance diffractometer with Cu $K\alpha_{1,2}$ radiation (Bruker-AXS) equipped with a position-sensitive X-ray detector (Lynxeye). A Sr-NTO (8 mol %) disc was rotated to record diffraction data in the 2θ range of 5−114° with a step of 0.016° and a total counting time of 840 s per step. TOPAS 5.0 software (Bruker-AXS) was used for the Rietveld structure refinement.[27−29]

3. RESULTS AND DISCUSSION

3.1. EXAFS of HCl-Washed Sr-NTO (50 mol %). Sr-NTO (50 mol %), the photocatalyst with the highest Sr concentration, exhibited the Sr K-edge spectrum with the best signal-to-noise ratio. To eliminate the possible contribution from Sr-containing residues that are soluble in HCl solution,

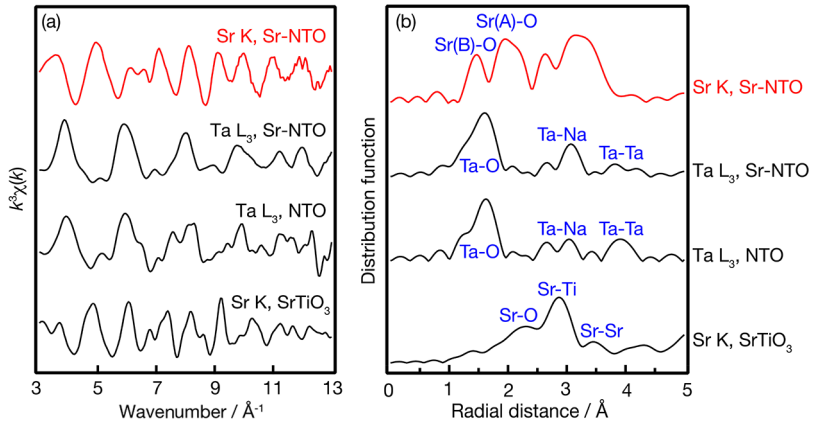

Figure 2. Extended X-ray absorption fine structures at the Sr K-edge and Ta L_3-edge observed for the HCl-washed Sr-NTO (50 mol %) photocatalyst. The Ta L_3-edge spectrum of NTO and Sr K-edge spectrum of $SrTiO_3$ are shown for reference. (a) k^3-weighted absorption spectra. (b) Radial distribution functions normalized to the height of the most intense peak. The k range in the Fourier transform was 3−13 $Å^{-1}$.

DOI: 10.1021/acscatal.7b03567
ACS Catal. 2018, 8, 880−885

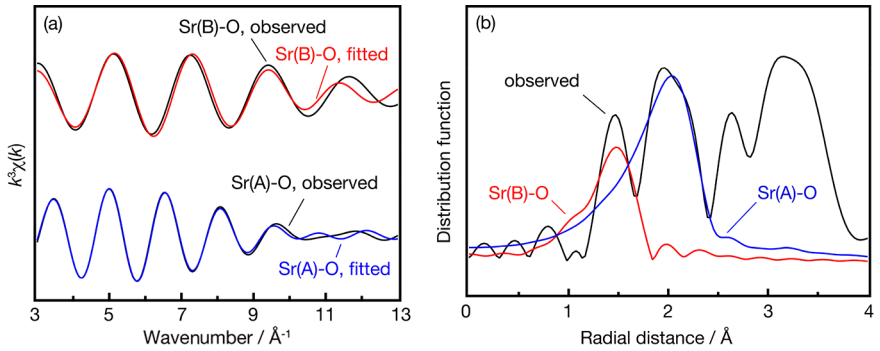

Figure 3. Results of curve fitting of the Sr K-edge spectrum of the HCl-washed Sr-NTO (50 mol %) photocatalyst. (a) Fourier-filtered and fitted k^3-weighted absorption spectra. (b) Observed and fitted radial distribution functions.

the HCl-washed photocatalyst was examined instead of Sr-NTO (50 mol %). Figure 2a shows the Sr K-edge EXAFS results for the HCl-washed photocatalyst. Fourier transformation of the k^3-weighted absorption spectrum yielded a radial distribution function with peaks at 1.5, 2.0, 2.6, and 3.1 Å (Figure 2b).

The peak at 1.5 Å corresponds to the Sr(B)−O shell with Sr cations at the B sites in $NaTaO_3$, which is supported by the Ta L_3-edge spectra of the same photocatalyst and of NTO (Figure 2). Radial distribution functions converted from the two Ta L_3-edge spectra peaked at 1.5 Å. Because Ta cations occupy the B sites in $NaTaO_3$, six O anions of each TaO_6 octahedron are the nearest-neighbor atoms to the Ta cation. Hence, the peak of the radial distribution at 1.5 Å provides evidence for the X-ray absorption of the M atom at the center of the MO_6 octahedron, which in this case refers to SrO_6, embedded in the host lattice. In the average cubic unit cell shown in Figure 1, the Ta−O distance in the TaO_6 octahedron is 1.95 Å. An apparent Sr(B)−O shell length of 1.5 Å is acceptable considering the phase shifts in the electron scattering by O anions.

The peak of the radial distribution at 2.0 Å is related to the Sr(A)−O shell with Sr cations at the A sites. Pristine $NaTaO_3$ includes NaO_{12} cuboctahedra with an average Na−O distance of 2.75 Å. By placing Sr cations at the centers of the cuboctahedra, a Sr−O shell can be observed at 2.0 Å in the radial distribution. The Sr K-edge EXAFS result for $SrTiO_3$ was used as a reference for the occupation of Sr at the A sites in a perovskite-structured metal oxide. The cubic cell length of $SrTiO_3$, 3.90 Å,[30] is identical to the average cell length of $NaTaO_3$. The radial distribution function shown in Figure 2b peaks at 2.2 Å. Similar Sr−O distances, i.e., 2.0 Å in Sr-NTO and 2.2 Å in $SrTiO_3$, indicate that SrO_{12} cuboctahedra are embedded in the two perovskite-structured compounds.

In the preceding paragraphs, we hypothesized that two Sr-containing local structures, i.e., a SrO_6 octahedron and a SrO_{12} cuboctahedron, are simultaneously present in Sr-NTO (50 mol %), in accordance with their radial distribution functions. Curve fitting was carried out to test our assumption and to quantify the lengths of the two shells. Oscillations in the absorption spectrum corresponding to the Sr(B)−O shell were isolated and filtered using a window function, followed by inverse Fourier transformation to afford the shell-related oscillations. The Fourier-filtered oscillations were fitted using one Sr−O shell with four adjustable parameters; shell length, coordination number, threshold energy difference, and squared displacement (Debye−Waller factor). Figure 3a shows the Fourier-filtered and best-fit oscillations. The radial distribution function deduced from the best-fit oscillations is compared with the original distribution in Figure 3b. Fitting with the Sr(A)−O shell was completed in the same manner using a filtering window tuned for this shell. Table 1 summarizes the refined parameters.

Table 1. Metal−Oxygen Shells in HCl-Washed Sr-NTO (50 mol %) and $SrTiO_3$[a]

shell	L/Å	CN	dE/eV	σ^2/Å^2	R range/Å
Sr(B)−O	1.96	1.1	−0.4	0.0065	1.12−1.72
Sr(A)−O	2.60	6.6	−3.8	0.0140	1.68−2.40
Ta−O	1.97	5.9	11.3	0.0091	1.12−1.72
Sr−O in $SrTiO_3$	2.80	15.0	3.2	0.0163	1.40−2.50

[a] L is the shell length; CN is the coordination number; dE is the threshold energy difference, σ^2 is the Debye−Waller factor, and R range is the filtering window for inverse Fourier transformation.

The Sr−O shell in $SrTiO_3$ and the Ta−O shell in Sr-NTO (50 mol %) were also fitted for reference. The Sr−O length in $SrTiO_3$, 2.76 Å,[30] and Ta−O length in the average lattice of $NaTaO_3$, 1.95 Å, were obtained in the refinement with precision better than 0.1 Å. The filtered and fitted oscillations of these reference shells are shown in Figures S2 and S3, respectively.

The most important issue here is the good fit for the two Sr−O shells. The residuals are satisfactorily small in k space (Figure 3a). Hence, the two Sr-containing local structures are simultaneously present in Sr-NTO (50 mol %). The use of EXAFS to characterize metal cations embedded in $NaTaO_3$ is thus feasible.

Doping of the B sites with Sr cations, which was concluded here, is possibly key to the enhancement of the quantum efficiency. The electron−hole recombination rate is controlled by the Sr concentration gradient in the Sr-NTO photocatalyst particles; a large gradient from the Sr-rich surface to the Sr-poor core leads to restricted recombination.[31] The conduction band of $NaTaO_3$ comprises Ta 5d orbitals.[32−34] By doping of the B sites with Sr cations, SrO_6 octahedra are embedded in the corner-shared network of the TaO_6 octahedra. The embedded octahedra hinder the overlap of the Ta 5d orbitals, which in turn narrows the conduction band with an upward shift of the band minimum. As a result, the light absorption edge for band-gap excitation is blue-shifted by doping with Sr.[22] The concentration gradient of the Sr cations at the B sites induces the energy gradient of the conduction band minimum. Hence, the band-gap-excited electrons, not holes, are driven by

DOI: 10.1021/acscatal.7b03567
ACS Catal. 2018, 8, 880−885

the energy gradient. Electrons are thereby separated from holes. This hypothesis is a promising mechanism for the enhancement of the quantum efficiency induced by the doping of metals.

The second issue is related to the shell lengths. The Sr(B)−O length is compatible with the Ta−O length in the same photocatalyst, indicating that the embedded SrO_6 octahedra are compressed in the surrounding $NaTaO_3$ lattice. The compressed SrO_6 octahedra induced marginal distortion in the surrounding lattice. Hence, the energy costs related to the occupation of Sr cations in the B sites can be limited. The SrO_6 octahedra in NaCl-structured SrO exhibited a Sr−O bond length of 2.57 Å. The Sr−O bond length in a diatomic SrO molecule is 1.92 Å.[35] Theoretical simulations should be conducted in the future to reveal the electronic structures induced by the compressed octahedra in Sr-NTO. The Sr(A)−O bond length decreased by 0.15 Å relative to the Na−O bond length in the average lattice of $NaTaO_3$. The stronger attractive electrostatic force in the $Sr^{2+}-O^{2-}$ ion pairs in comparison with that in the $Na^{+}-O^{2-}$ pairs decreased the ion-pair length.

The coordination numbers are another issue. In pristine $NaTaO_3$, the A- and B-site cations are coordinated by 12 and 6 O anions, respectively. If the same number of Na and Ta cations were exchanged with Sr cations, the coordination number of the Sr(A)−O shell would be twice the coordination number of the Sr(B)−O shell. However, this was not observed. The ratio of the coordination numbers was 6 instead of 2 (Table 1). When we assumed that Sr cations alternatively occupy the A or B sites, the coordination number obtained by curve fitting is proportional to the number of Sr cations at each type of site. According to this assumption, the observed ratio predicts a cation number ratio of three Sr cations at A sites per one Sr cation at a B site. This number ratio is in agreement with the composition of $NaTaO_3$–$Sr(Sr_{1/3}Ta_{2/3})O_3$ solid solution. $Sr(Sr_{1/3}Ta_{2/3})O_3$ is a known compound,[36,37] and its solid solution with $NaTaO_3$ explains the simultaneous presence of the Sr cations at the A and B sites with no need to create oxygen anion vacancies to balance cationic and anionic charges.

Two more peaks, i.e., one small peak at 2.6 Å and one large peak at 3.1 Å, can be observed in the radial distribution function of Sr-NTO (50 mol %) (Figure 2a). In pristine $NaTaO_3$, each Na cation is coordinated by eight Ta cations with an average Na−Ta distance of 3.37 Å. On the other hand, each Ta cation is coordinated by eight Na cations with the same distance. After simultaneous placement of Sr cations at the A and B sites, Sr(A)−Ta and Sr(B)−Na shells were observed instead of Na−Ta and Ta−Na shells. The two shells with different scattering atoms incidentally produced one peak or one pair of peaks in the radial distribution function. It is difficult to fit the spectrum with a single shell. Hence, fitting by one Sr(A)−Ta shell is possible under the assumption that Ta cations dominate the electron scattering in Sr-NTO. Figure S4 and Table S1 show the results obtained from curve fitting on the basis of this assumption.

Nearest Ta−Ta neighbors were examined in the Ta L_3-edge EXAFS of NTO and Sr-NTO (50 mol %) to confirm the assignment of the other shells conducted above. The two photocatalysts exhibited Ta−Ta bond lengths of 3.98 and 4.02 Å, which are consistent with the unit cell length of $NaTaO_3$. Figures S5 and S6 and Tables S2 and S3 show the results obtained from curve fitting.

3.2. EXAFS of Sr-NTO with Low Sr Concentrations.

HCl-washed Sr-NTO (50 mol %), the photocatalyst with the highest Sr concentration examined herein, contains Sr cations at the A and B sites, as concluded in the preceding subsection. However, the Sr concentrations for the best water-splitting efficiency were considerably less than 50 mol %. Iwase et al.[4] examined the overall water-splitting reaction using Sr-NTO with Sr concentrations of 0.1−8 mol % and reported an optimum rate for H_2 and O_2 production at 0.5 mol % in the presence of a NiO cocatalyst. An and Onishi[22] examined the rate of electron−hole recombination in Sr-NTO as a function of the Sr concentration and found a minimum rate at 1.8 mol %. Hence, Sr-NTO with lower Sr concentrations (2 and 20 mol %) should be characterized.

Figure 4 shows the Sr K-edge EXAFS of Sr-NTO (2 mol %), Sr-NTO (20 mol %), and HCl-washed Sr-NTO (50 mol %).

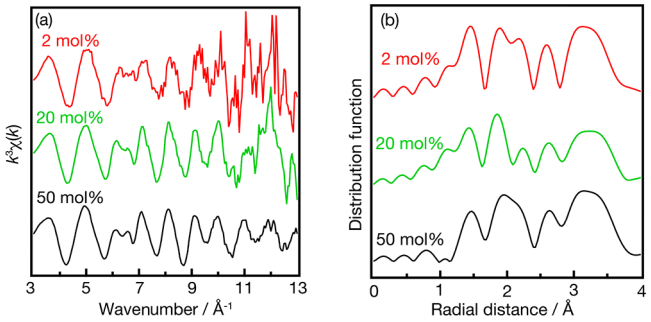

Figure 4. Extended X-ray absorption fine structures at the Sr K-edge observed for the Sr-NTO photocatalysts prepared herein. (a) k^3-weighted absorption spectra. (b) Radial distribution functions normalized to the height of the most intense peak. The k range in the Fourier transform was 3−13 Å^{-1}.

The k^3-weighted absorption spectra of the three Sr-NTOs were identical, as shown in panel (a), while the signal-to-noise ratio accordingly decreased. Hence, the radial distribution functions in panel (b) are not sensitive to the Sr concentration. These results indicate that the local coordination around Sr cations is not sensitive to the Sr concentration. The A and B sites of $NaTaO_3$ are doubly doped with Sr cations even in the photocatalysts with low Sr concentrations.

3.3. X-ray Absorption Near-Edge Structures of Sr-NTO.

Figure 5 shows the near-edge structures at the Sr K-edge

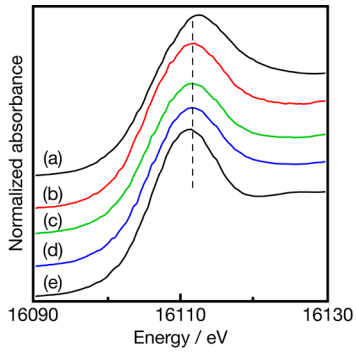

Figure 5. Near-edge structures of Sr-doped $NaTaO_3$ photocatalysts and related compounds: (a) SrO, (b) Sr-NTO (2 mol %), (c) Sr-NTO (8 mol %), (d) Sr-NTO (20 mol %), and (e) $SrTiO_3$. The dashed line represents the peak energy of Sr-NTO. The absorbance was normalized to the peak of each spectrum.

DOI: 10.1021/acscatal.7b03567
ACS Catal. 2018, 8, 880−885

observed for the three Sr-NTO photocatalysts and two reference compounds, SrO and $SrTiO_3$. The photocatalysts exhibited a common spectrum with different intensities, with the absorption peak at 16 111 eV. The common spectrum was consistent with the insensitivity of the local Sr coordination to the Sr concentration as indicated by EXAFS. SrO with SrO_6 octahedra produced a peak at an energy greater than 16 111 eV, whereas $SrTiO_3$ with SrO_{12} cuboctahedra produced a lower-energy peak. With the simultaneous occupation of the Sr cations at the A and B sites in Sr-NTO, the absorption peak was naturally observed between the two peaks of SrO and $SrTiO_3$.

3.4. Rietveld Analysis. The coordination numbers obtained in EXAFS confirmed the formation of the $NaTaO_3$–$Sr(Sr_{1/3}Ta_{2/3})O_3$ solid solution in Sr-NTO. Rietveld analysis of the XRD data for Sr-NTO (8 mol %) was carried out to verify the formation of the solid solution. Refinement started from the orthorhombic structure of pristine $NaTaO_3$[25] with occupation of the Sr cations at the A and B sites. For the refinement of the fractional coordinates, special positions were held constant, and all of the other general positions were refined. The occupancies of Ta and Sr at the 4a sites and of Na and Sr at the 4c sites were constrained to meet the chemical formula $Sr_xNa_{1-x}(Sr_{x/3}Ta_{1-x/3})O_3$, with the occupancy of Sr at the 4c site as the free fitting parameter. The oxygen occupancy was held to be unity. The introduction of a preferred orientation along [001] was mandatory. In addition, the thermal parameters were refined.

Figure 6 shows the observed and refined patterns. A good fit was obtained, as evidenced by an *R* Bragg value of 1.9 and a goodness-of-fit indicator of 4.2. Table 2 summarizes the refined parameters. The refined unit cell lengths were a = 5.5510 (0.0004) Å, b = 5.5032 (0.0003) Å, and c = 7.7904 (0.0003) Å (the numbers within parentheses represent the estimated errors). The occupation of Sr at the B sites was 0.024, and that at the A sites was 0.073, which led to an overall Sr concentration of 9.7 mol % relative to Ta. This number is in agreement with the composition determined by X-ray fluorescence, i.e., 8.3 mol %. Hence, the $NaTaO_3$–$Sr(Sr_{1/3}Ta_{2/3})O_3$ solid solution in Sr-NTO photocatalysts is supported by Rietveld analysis.

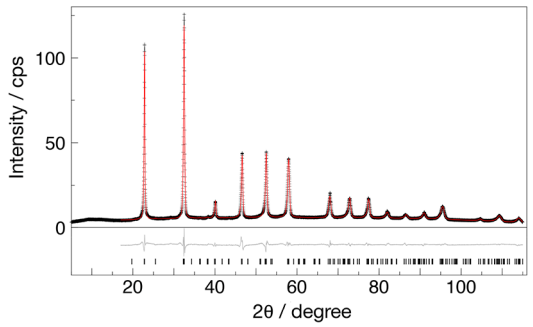

Figure 6. XRD patterns of Sr-NTO (8 mol %). Black crosses, observed pattern; red line, calculated pattern; gray line, difference between the two. Vertical bars at the bottom indicate the peak positions.

Table 2. Rietveld-Refined Parameters for the Sr-NTO (8 mol %) Photocatalyst[a]

atom	site	N	occ.	x	y	z	B/Å^2
Ta(B)	4a	4	0.976	0	0	0	0.29
Sr(B)	4a	4	0.024	0	0	0	2.00
Na(A)	4c	4	0.927	−0.017	0.473	0.250	0.01
Sr(A)	4c	4	0.073	−0.017	0.473	0.250	1.70
O	8d	8	1	0.206	0.253	0.042	0.01
O	4c	4	1	0.005	0.026	0.250	0.01

[a]N is the number of equivalent atoms; occ. is the fractional occupation; x, y, and z are the atom coordinates in the unit cell vector length; B is the isotropic displacement parameter.

4. CONCLUSIONS

Doping with Sr cations by a solid-state reaction leads to simultaneous occupation of the A and B sites of perovskite-structured $NaTaO_3$ by Sr. The EXAFS at the Sr K-edge reveals the presence of two Sr–O shells in the photocatalysts doped at 2, 20, and 50 mol %. The Sr–O bond length in each shell in the photocatalyst doped at 50 mol % was quantified by curve fitting. The small shell with a Sr–O bond length of 1.96 Å corresponds to SrO_6 octahedra with Sr cations at the B sites. This length is compatible with the Ta–O bond length in the TaO_6 octahedra, indicating that the surrounding $NaTaO_3$ lattice compressed the SrO_6 octahedra. The other shell with a Sr–O bond length of 2.60 Å corresponds to SrO_{12} cuboctahedra with Sr cations at the A sites. The resulting $NaTaO_3$–$Sr(Sr_{1/3}Ta_{2/3})O_3$ solid solution accommodates the Sr cations with no requirement for oxygen anion vacancies, as evidenced by the Rietveld refinement of XRD data and the coordination numbers obtained from EXAFS. We therefore propose that SrO_6 octahedra embedded in the corner-shared network of the TaO_6 octahedra are crucial to the enhancement of the quantum efficiency via doping of $NaTaO_3$ photocatalysts with Sr.

■ ASSOCIATED CONTENT

Supporting Information

The Supporting Information is available free of charge on the ACS Publications website at DOI: 10.1021/acscatal.7b03567.

XRD patterns for all of the photocatalysts and XAFS details (PDF)

■ AUTHOR INFORMATION

Corresponding Author

*E-mail: oni@kobe-u.ac.jp.

ORCID

Christof Wöll: 0000-0003-1078-3304

Hiroshi Onishi: 0000-0003-1873-9105

Notes

The authors declare no competing financial interest.

■ ACKNOWLEDGMENTS

This study was supported by JSPS KAKENHI Grant JP16H02250. X-ray absorption measurements were performed under the approval of the Photon Factory Program Advisory Committee (Proposal 2016G057).

■ REFERENCES

(1) Kudo, H.; Kato, H. *Chem. Phys. Lett.* **2000**, *331*, 373–377.
(2) Kato, H.; Asakura, K.; Kudo, H. *J. Am. Chem. Soc.* **2003**, *125*, 3082–3089.

DOI: 10.1021/acscatal.7b03567
ACS Catal. 2018, 8, 880–885

(3) Iwase, A.; Kato, H.; Okutomi, H.; Kudo, A. *Chem. Lett.* **2004**, *33*, 1260−1261.
(4) Iwase, A.; Kato, H.; Kudo, A. *ChemSusChem* **2009**, *2*, 873−877.
(5) Kudo, A.; Niishiro, R.; Iwase, A.; Kato, H. *Chem. Phys.* **2007**, *339*, 104−110.
(6) Yi, Z. G.; Ye, J. H. *Appl. Phys. Lett.* **2007**, *91*, 254108.
(7) Iwase, A.; Saito, K.; Kudo, A. *Bull. Chem. Soc. Jpn.* **2009**, *82*, 514−518.
(8) Yang, M.; Huang, X.; Yan, S.; Li, Z.; Yu, T.; Zou, Z. *Mater. Chem. Phys.* **2010**, *121*, 506−510.
(9) Kanhere, P.; Nisar, J.; Tang, Y.; Pathak, B.; Ahuja, R.; Zheng, J.; Chen, Z. *J. Phys. Chem. C* **2012**, *116*, 22767−22773.
(10) Kang, H. W.; Lim, S. N.; Park, S. B.; Park, A.-H. A. *Int. J. Hydrogen Energy* **2013**, *38*, 6323−6334.
(11) Yamashita, D.; Takata, T.; Hara, M.; Kondo, J. N.; Domen, K. *Solid State Ionics* **2004**, *172*, 591−595.
(12) Higashi, M.; Abe, R.; Teramura, K.; Takata, T.; Ohtani, B.; Domen, K. *Chem. Phys. Lett.* **2008**, *452*, 120−123.
(13) Zhao, Z.; Li, R.; Li, Z.; Zou, Z. *J. Phys. D: Appl. Phys.* **2011**, *44*, 165401.
(14) Balaz, S.; Porter, S. H.; Woodward, P. M.; Brillson, L. J. *Chem. Mater.* **2013**, *25*, 3337−3343.
(15) Higashi, M.; Domen, K.; Abe, R. *J. Am. Chem. Soc.* **2013**, *135*, 10238−20241.
(16) Ueda, K.; Kato, H.; Kobayashi, M.; Hara, M.; Kakihana, M. *J. Mater. Chem. A* **2013**, *1*, 3667−3674.
(17) Modak, B.; Srinivasu, K.; Ghosh, S. K. *J. Phys. Chem. C* **2014**, *118*, 10711−10719.
(18) Si, W.; Pergolesi, D.; Haydous, F.; Fluri, A.; Wokaun, A.; Lippert, T. *Phys. Chem. Chem. Phys.* **2017**, *19*, 656−662.
(19) Teramura, K.; Okuoka, S.-i.; Tsuneoka, H.; Shishido, T.; Tanaka, T. *Appl. Catal., B* **2010**, *96*, 565−568.
(20) Jeyalakshmi, V.; Mahalakshmy, R.; Krishnamurthy, K. R.; Viswanathan, B. *Catal. Today* **2016**, *266*, 160−167.
(21) Nakanishi, H.; Iizuka, K.; Takayama, T.; Iwase, A.; Kudo, A. *ChemSusChem* **2017**, *10*, 112−118.
(22) An, L.; Onishi, H. *ACS Catal.* **2015**, *5*, 3196−3206.
(23) Shimura, K.; Kato, S.; Yoshida, T.; Itoh, H.; Hattori, T.; Yoshida, H. *J. Phys. Chem. C* **2010**, *114*, 3493−3503.
(24) Husin, H.; Su, W.-N.; Chen, H.-M.; Pan, C.-J.; Chang, S.-H.; Rick, J.; Chuang, W.-T.; Sheu, H.-S.; Hwang, B.-J. *Green Chem.* **2011**, *13*, 1745−1754.
(25) Kennedy, B. J.; Prodjosantoso, A. K.; Howard, C. J. *J. Phys.: Condens. Matter* **1999**, *11*, 6319−6327.
(26) Ravel, B.; Newville, M. *J. Synchrotron Radiat.* **2005**, *12*, 537−541.
(27) *TOPAS V4 User's Manual*; Bruker AXS: Karlsruhe, Germany, 2008.
(28) Cheary, R. W.; Coelho, A. A. *J. Appl. Crystallogr.* **1992**, *25*, 109−121.
(29) Rietveld, H. M. *J. Appl. Crystallogr.* **1969**, *2*, 65−71.
(30) Abramov, Y. A.; Tsirelson, V. G.; Zavodnik, V. E.; Ivanov, S. A.; Brown, I. D. *Acta Crystallogr., Sect. B: Struct. Sci.* **1995**, *51*, 942−951.
(31) An, L.; Park, Y.; Sohn, Y.; Onishi. *J. Phys. Chem. C* **2015**, *119*, 28440−28447.
(32) Choi, M.; Oba, F.; Tanaka, I. *Phys. Rev. B: Condens. Matter Mater. Phys.* **2008**, *78*, 014115.
(33) Wang, H.; Wu, F.; Jiang, H. *J. Phys. Chem. C* **2011**, *115*, 16180−16186.
(34) Modak, B.; Srinivasu, K.; Ghosh, S. K. *J. Phys. Chem. C* **2014**, *118*, 10711−10719.
(35) *CRC Handbook of Chemistry and Physics*, 92nd ed.; CRC Press: Boca Raton, FL, 2011; pp 9−29.
(36) Yoshioka, K.; Petrykin, V.; Kakihana, M.; Kato, H.; Kudo, A. *J. Catal.* **2005**, *232*, 102−107.
(37) Caldes, M. T.; Deniard, P.; Zou, X. D.; Marchand, R.; Diot, N.; Brec, R. *Micron* **2001**, *32*, 497−507.

DOI: 10.1021/acscatal.7b03567
ACS Catal. 2018, 8, 880−885